Inductive Sintering of Silver Micro Particles for Bonding of Microelectronic Components

Patrick Rochala *, Christian Hofmann, Martin Kroll, Sushant Panhale, Rezan Javed, Karla Hiller

Posted Date: 26 June 2023

doi: 10.20944/preprints202306.1796.v1

Keywords: Induction heating; rapid heating; power electronics; die-attach; chip bonding; power electronic packaging; electromagnetic field; (silver) sintering; particle bonding; DBC

Article

Inductive Sintering of Silver Micro Particles for Bonding of Microelectronic Components

Patrick Rochala [1]*, Christian Hofmann [2]*, Martin Kroll [1]*, Sushant Panhale [1], Rezan Javed [3] and Karla Hiller [4]

[1] Institute for Machine Tools and Production Processes (IWP), Professorship for Forming and Joining, Chemnitz University of Technology, 09126 Chemnitz, Germany; patrick.rochala@mb.tu-chemnitz.de (P.R.), martin.kroll@mb.tu-chemnitz.de (M.K.), Sushant.panhale@mb.tu-chemnitz.de (S.P.)

[2] Fraunhofer Institute for Electronic Nano Systems ENAS, 09126 Chemnitz, Germany; christian.hofmann@enas.fraunhofer.de (C.H.)

[3] Institute of Lightweight Structures, Professorship for Lightweight Structures and Polymer Technology, Chemnitz University of Technology, 09126 Chemnitz, Germany; rezan.javed@mb.tu-chemnitz.de (R.J.)

[4] Center for Microtechnologies, Chemnitz University of Technology, 09126 Chemnitz, Germany; karla.hiller@zfm.tu-chemnitz.de (K.H.)

* Correspondence: P.R.; C.H.; M.K.

Abstract: In this article, an efficient die bonding technology based on silver sintering due to induction heating is presented. By using this technology, the heat for the sintering reaction is locally limited to the bonding area and the heating of the entire power module is avoided. Furthermore, the sintering reaction is promoted due to current flow between the silver particles and the sintering time is drastically reduced. Next to the experimental trials presented in this paper, FE-simulation methods were applied in order to develop a suitable induction coil geometry for the bonding of a diode to a direct bonded copper (DBC) substrate. Additional heating and sintering tests verified the reliability of the simulation model as well as the technological approach. Diodes were successfully bonded during the experiments and were analyzed by means of scanning electron microscopy (SEM) and function tests in order to qualify the inductive bonding technology. The results presented in this paper demonstrate, that induction heating has high potential for cost effective production in the field of die-attach and can drastically increase the output in power electronics production.

Keywords: Induction heating; rapid heating; power electronics; die-attach; chip bonding; power electronic packaging; electromagnetic field; (silver) sintering; particle bonding; DBC

1. Introduction

1.1. Scientific-technologic Background

Power electronics represent a core area of the technological development of the 21st century [1] as power modules are essential in numerous key applications, e.g. in drives for hybrid, electric and rail vehicles, in converters for photovoltaic and wind energy plants as well as in devices of energy storage and distribution. The main elements of power electronic systems are base plate, DBC substrate, heat sink, housing and power electronic component. Wire bonds or ribbon bonds are used to electrically connect the power electronic components with each other and with the circuit board. For heat dissipation purposes, a thermal interface material is usually placed between power electronic device and heat sink. Typical power electronic components (discrete dies) are e.g. diodes, IGBTs (Insulated Gate Bipolar Transistor), MOSFETs (Metal-Oxide-Semiconductor Field-Effect Transistor), bipolar transistors and power-LEDs. The die-attach process bonds the power electronic component to

 doi:10.20944/preprints202306.1796.v1

the DBC substrate, which has huge impact on reliability and performance of the power module. It establishes the mechanical, thermal and electrical connection between power electronic component and substrate and needs to be fast, efficient and safe in application. Additionally, the packaging method is not allowed to inflict a high amount of thermal stress on the power electronic components. Furthermore, the produced bonds need to be free of voids, cracks and other defects. As a result, there is a high demand for innovation in the field of die-attach technology that serves the requirements stated above [1]–[3].

Power electronic components are usually bonded to copper metallized ceramic substrates (Al_2O_3, AlN, Si_3N_4). For this purpose, soldering and diffusion soldering, as low temperature bonding techniques, are state of the art in die-attach applications. The homologous temperature T_{hom} is an important factor that allows to qualify the thermal and long term mechanical stability of the bond and is defined as the ratio of the melting temperature of the bonding material T_m and the application temperature of the bonded device during service T_{app}:

$$T_{hom} = \frac{T_{app}}{T_m} \qquad (1)$$

Low melting Sn-Ag solders exhibit high homologous temperatures and cannot endure high operational temperatures because the homologous temperature is not allowed to exceed 0.8 in order to avoid re-melting of the interface. From the literature, it is also known that for homologous temperatures of 0.4 and above, creep effects are commonly expected [4]. With regard to an increasing number of high power density applications of power modules, especially in the field of automotive production, these modules are often used at elevated ambient temperatures. Wide-bandgap semiconductor devices made of SiC or GaN have very good electrical properties, can endure very high switching frequencies, voltages and power levels and can be operated at temperatures up to 300 °C without damage. As a result, in the field of power electronics, bonding materials are needed on the one hand to have a low bonding temperature in order to prevent the semiconductor components from damage during bonding, but on the other hand, a high re-melting temperature is also required. Thus, bonding materials with low homologous temperatures are needed. Additionally, low bonding temperatures reduce production costs due to less power consumption during the bonding process. It is a technological challenge to design such materials that serve these diametrical requirements.

Another state of the art bonding method is diffusion soldering. For this technique, Sn-based solders are also used, but the bonding process strongly relies on interdiffusion effects. By controlling the bonding process parameters, high-melting intermetallic phases are formed throughout the entire bonded interface, whereas for soldering, the interface mainly consists of the bond material in its original state and only a thin intermetallic layer can be found at the interface [5]. The composition of the intermetallics in the diffusion bonded interface depends on the solder materials used as well as the chip and the sort of ceramic substrate metallization. As a result, the interfaces exhibit high homologous temperatures. As an example, for Cu-Sn bonded stacks, assuming that the service temperature is T_{app} = 300 °C, homologous temperatures in the range of $0.52 \leq T_{hom} \leq 0.65$ can be achieved, depending on the metallurgical composition of the interface [5]. In order to establish a fast and productive diffusion bonding process, optimized process parameters are needed and a firm contact between bond material and chip as well as substrate is required.

The bonding via sintering of micro- and nanoscale silver particles is becoming increasingly important, because highly temperature stable interfaces can be produced. In most cases, the particles are dispersed in an organic vehicle and thus have a paste-like appearance which allows to apply the particles to the bonding surface. During the bonding process, the silver material does not melt and the bond is primarily established by means of silver interdiffusion, which leads to an increasing coalescence of the particles (cohesion) as well as bonding of the particles to the substrate (adhesion). After bonding, a porous interface is established that is firmly bonded to the bonding partners. A defined bonding temperature as well as a bonding pressure drives the sintering reaction. A more detailed description of the sintering process is given in section 1.2.

Advantages of silver sintering are the comparatively low temperatures during the bonding process [6] and the high thermal stability of the sintered interfaces. As the interfaces exhibit the re-melting temperature of pure silver (T_m = 961.8 °C), homologous temperatures of T_{hom} = 0.46 can be achieved for a maximum service temperature of T_{app} = 300 °C. Further advantages of sintered bonds are their superior thermal conductivity [7], [8] and good mechanical properties [9], [10]. Currently, micro-scaled silver particles are commonly used [9], [11], [12] but a growing number of publications are reporting on the application of nano-scale silver particles as bonding material [13]–[16] as these materials allow for even lower sintering temperatures due to smaller particle diameters and less energy consumption for promoting the sinter reaction.

Because silver sintering is becoming more and more state of the art in die-attach bonding, a huge number of scientific publications focus on this topic. Besides numerous investigations on process parameters and their impact on mechanical and thermal properties of the bond in dependence of the material system of the stack, many studies try to widen the application potential of silver sintering materials. Until now, silver particles were mostly used to bond power electronic components on copper or silver surfaces, but there are also quite promising results for bonding on nickel [15], [17]and gold [15]surfaces. With the increasing demand for power electronics, sintering numerous semiconductor devices in one process step is important by means of high productivity. The sintering on large surfaces is not trivial, because large area bonds pose a challenge with regard to degassing of the organics in the interface and the increased mechanical load on the stack due to high bonding forces. As a result, adjusted strategies for pre-drying and pressureless bonding are needed [13], [15], [16].

In most cases, the process heat for the sintering process is provided by global heating of the parts by means of heat convection or conduction, for example in a sintering press with a hot plate or in an furnace. Induction heating is another method that is widely used as heat source in macro-scale applications like hardening, soldering and metal melting but is rarely used in die-attach applications. Thus, induction based bonding is almost nonexistent in the literature, although induction heating is very energy efficient, fast and allows to locally limit the heat generation to the bond zone. Sosnowchik et al. [18] successfully bonded micro-electro-mechanical systems (MEMS) based strain sensors to steel by induction heating within 3 to 5 seconds of bonding time using a low melting Sn-Ag eutectic solder layer, reporting that the heat input could be limited to some several micrometers below the steel surface at the bond zone. The bonds showed excellent mechanical characteristics. Yang et al. presented results for selective induction heating of micro scale structures with a thicknesses ranging from $20 \leq d \leq 60$ [µm] and a surface area of $9 \leq A \leq 16$ [mm²], stating that the shape of the structures has the biggest impact on their heatability [19]. In the article, the authors emphasize once again the very high heating rates of induction technology as well as the possibility to locally limit the heat input. Hofmann et al. successfully realized a MEMS packaging method based on selective induction heating of Cu-Sn layers for energy-efficient bonding at chip and wafer level using miniaturized coils with optimized geometry designs [20], [21]. Even less literature is available for induction based silver sintering. Guyon et al. [22] inductively heated nickel and silver powders with particle diameters ranging from $2 \leq d_P \leq 30$ [µm] and investigated the densification of the sintered structures, comparing them to conventionally sintered structures of the same powder. The authors were able to show, that for Ni powders a higher densification of the sintered structure could be achieved via induction heating, assuming that the powder densification is faster because of higher diffusion rates due to the induced eddy currents in the particles. This phenomenon could not be observed for the much coarser silver powder used in the study. However, the swelling phenomenon, that is characteristic for silver sintering, causing the volume of the sintered structure to slightly increase during heating due to rising gas pressure in the pores, was reduced. The cited results show, that induction based sintering could potentially increase the quality of the sintered structures due to improved densification in the sintering process. With adjusted silver particle sizes and induction parameters, the aforementioned effect of an accelerated densification of the sintered structure could potentially be exploited in die-attach applications in order to produce tough and temperature resistant bonds. It seems likely, the

 doi:10.20944/preprints202306.1796.v1

authors of the present paper are the only ones that published research on induction based silver sintering for power electronics fabrication [23]–[25].

1.2. Physical Background

According to Ampère's law, a current-carrying primary conductor generates a magnetic field, of which the field strength is primarily dependent of the current in the conductor. Hence, for alternating currents, an alternating magnetic field is generated and an electrically conductive component that is placed within this field is inductively heated. This is due to an alternating current that is induced in the component, which acts as a secondary conductor. The induced current has the same frequency as the electromagnetic excitation field but the direction of the current flow is opposite to its cause. Consequently, eddy currents are generated in the component, which produce heat due to the electrical resistance of the component's material (Ohm's law). Furthermore, the heating happens immediately due to the intrinsic heat generation because of the material's resistivity.

The aim of the conducted investigations presented in this paper is to generate the necessary process temperature for die-attach by means of silver sintering with high-frequency electromagnetic fields, whereby the heat input is limited to the bond zone. Ideally, only the silver sinter layer is heated. The inductively generated thermal energy is used to sinter the silver particles, which means that the particles fuse in solid state and grow to larger structures. During this process, a densified sinter layer is generated and a firm joint between sinter layer and substrate as well as the power electronic component is established due to sintering of the silver particles to the corresponding metallic interface. Up to now, induction technology is barely used in the field of die-attach, but it holds great potential for making bonding processes faster and more efficient.

In their initial state, the silver particles have a high surface-to-volume ratio and thus possess a very high surface energy, so that they strive to reduce their volume by coalescing. By applying thermal energy and a bonding pressure, the sintering reaction of the particles with each other and with an adjacent metallic substrate is initiated. During this process, the sintered structure becomes increasingly dense and the bond to the substrate is strengthened, too. Due to the particles' intrinsic need to grow together, it is possible to sinter at comparatively low process temperatures. Once the particles have been sintered, the re-melting temperature of the structure corresponds to that of pure silver, which is the reason for the high thermal stability of the sintered layers. In the case of sintering by means of inductive heating, it was observed that the sintering reaction proceeds very quickly and the densification of the layers is very pronounced [23]. The reason for this is that during induction heating, eddy currents are induced inside the particles which also flow between adjacent particles. As a result, particularly strong heating occurs at the contact points due to the contact resistance. As the sintering reaction and the densification of the particles progress, neck growth between particles occurs and thus the contact points between the particles increase in size. This reduces the intensity of induction heating due to reduced contact resistance and the heat input into the sinter layer decreases. Thus, the inductive sintering process regulates itself. In addition to the current-driven effect of heating, several thermal effects that are characteristic in field-assisted sintering, can accelerate the sintering process as well [26].

In this paper, a technology is presented, which utilizes quick induction heating for silver sintering as bonding method. Comparatively low process temperatures and locally limited heat input are further advantages of this technology while at the same time the established bonds have the positive property profiles mentioned above.

2. Materials and Methods

2.1. Materials and Process Design

Diodes and direct bonded copper (DBC) substrates were used as bonding partners for the inductive die-attach process based on silver sintering. The diodes have a chip size of A_D = 9.0 x 9.0

Preprints (www.preprints.org) | NOT PEER-REVIEWED | Posted: 26 June 2023 doi:10.20944/preprints202306.1796.v1

mm² and a total thickness of $h_D \approx 120$ µm. The pad metallization of the chip front side consists of an aluminum/silicon/copper layer system and the backside or bond surface is metallized with a nickel/silver layer. Figure 1 shows the diode with SEM cross sections of the front side (a) and backside (b).

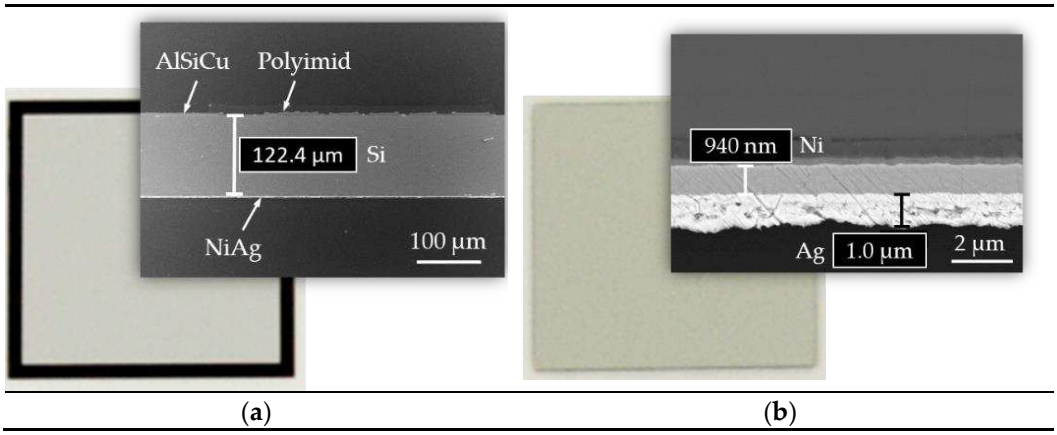

Figure 1. Diode before chip bonding: (**a**) Photographic image and SEM cross-section of the front side; (**b**) Photographic image and SEM cross section of the back side.

The DBC substrate has a length of $l_{DBC} = 53$ mm and a width of $w_{DBC} = 39$ mm. The core of the DBC substrate is an aluminum oxide (Al_2O_3) ceramic with an approximate thickness of $h_{Al2O3} = 400$ µm. The ceramic is coated with a copper metallization ($h_{Cu} \approx 300$ µm) on the front and backside. The DBC substrate with a cross section through the entire layer stack is shown in Figure 2.

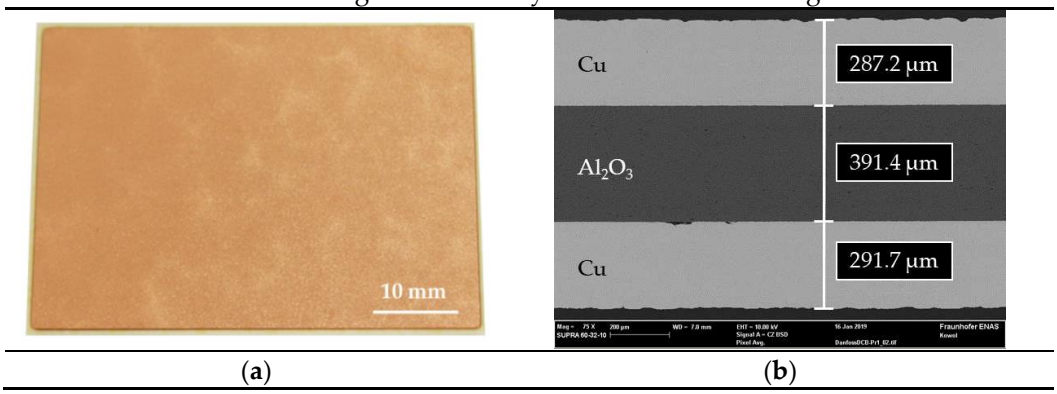

Figure 2. DBC substrate before chip bonding: (**a**) Photographic image of the copper-metallized bond surface; (**b**) Cross-sectional view of the DBC substrate with the Cu-Al_2O_3-Cu stack.

The silver-based particle paste ASP 043-04 from Heraeus Electronics, Germany was used as bond material, which is suitable for die-attach in power electronic applications. The paste has a silver content of $V_{Ag} = 85$ wt% and a maximum silver particle diameter of $D_{Ag} \leq 20$ µm. According to the manufacturer, it is fully compatible with chemically inert bond surfaces (e.g. silver, gold). Based on the technical data sheet, a compatibility with copper surfaces is expected and its evaluation is part of the inductive sintering experiments in the present paper. For the preparation of the experiments, a single paste pad with the size of $A_{Ag} = 10.0 \times 10.0$ [mm] was printed in the center of the DBC substrate directly onto the copper layer using stencil printing. For this purpose, a stencil with a thickness of 50 µm was used. Subsequently, the pad was pre-dried at a temperature of $T_D \leq 110$ °C for $t_D = 10$ min in a laboratory oven. The average thickness of the pre-dried silver layer with consideration of the shrinkage was $h_{Ag\_\varnothing} = 28.6$ µm. Finally, the diodes were placed on top of the silver pads for the inductive sintering experiments. The setup comprising the DBC, the silver sinter layer, and diode is referred to "stack" in the further course of the paper.

Preprints (www.preprints.org) | NOT PEER-REVIEWED | Posted: 26 June 2023 doi:10.20944/preprints202306.1796.v1

Based on the technical data sheet, a sintering temperature of $T_S \geq 230$ °C and a bonding pressure of $p \geq 10$ MPa are required. The upper temperature limit for bonding was set to $T = 350$ °C in order to protect the diodes from damage. A detailed description of the experimental setup and the bonding process is presented in subchapter 2.3. A summarized overview of the most relevant dimensions and material parameters of the bonding setup is given in Table 1.

Table 1. Material and design parameters of the bond substrates.

	Symbol	Unit	Value
Diode			
Length	l_D	mm	9.0
Width	w_D	mm	9.0
Thickness	d_D	µm	120.0
Bond metallization: Thickness Ni	d_{Ni}	µm	approx. 1
Bond metallization: Thickness Ag	d_{Ag}	µm	approx. 1
DBC substrate			
Length	l_D	mm	53.0
Width	w_D	mm	39.0
Thickness aluminum oxide	h_{Al2O3}	µm	approx. 400.0
Thickness copper	h_{Cu}	µm	approx. 300.0
Ag paste pad			
Pad length	l_{Ag}	mm	10.0
Pad width	w_{Ag}	mm	10.0
Pad thickness after pre-drying	$h_{Ag\_Ø}$	µm	28.6
Ag particle diameter	D_{Ag}	µm	≤ 20
Silver content	V_{Ag}	wt%	85.0

2.2. Simulation Method and Model

Numerical simulation by finite element method (FEM) is used to represent the inductive heating process as well as the die-attach. Consequently, using the material characteristics and the current parameters, the heating behavior of the individual components (especially of the sintered layer) is to be calculated and potential component damage can be virtually estimated and prevented. The aim of the simulation studies was the development of a coil geometry adapted to the sintering application, which should facilitate local heating primarily in the bond area as well as within the silver particle layer. Consequently, surrounding areas should remain at a lower temperature so that the thermal load on the DBC substrate and the power electronic component is reduced. For this purpose, the simulation software COMSOL Multiphysics with the AC/DC and heat transfer module was used. The simulation model consists of the DBC substrate with the silver sintered layer and the diode (assumed as pure silicon) placed on the silver layer, a silicon nitride (SiN) punch, a support plate made of the mineral composite material GL®P (Brandenburger Isoliertechnik GmbH & Co. KG, Germany) and the surrounding air. All components were simplified modeled using CAD tools and arranged in relation to each other according to the bonding tests. The simulation model was supplemented by the copper induction coil, which was geometrically adjusted in several iteration steps to achieve the maximum heat concentration in the bond zone. The geometric model of the simulation can be seen in Figure 3. Finally, material properties were assigned to the individual geometric components of the simulation model according to Table 2.

Preprints (www.preprints.org) | NOT PEER-REVIEWED | Posted: 26 June 2023 doi:10.20944/preprints202306.1796.v1

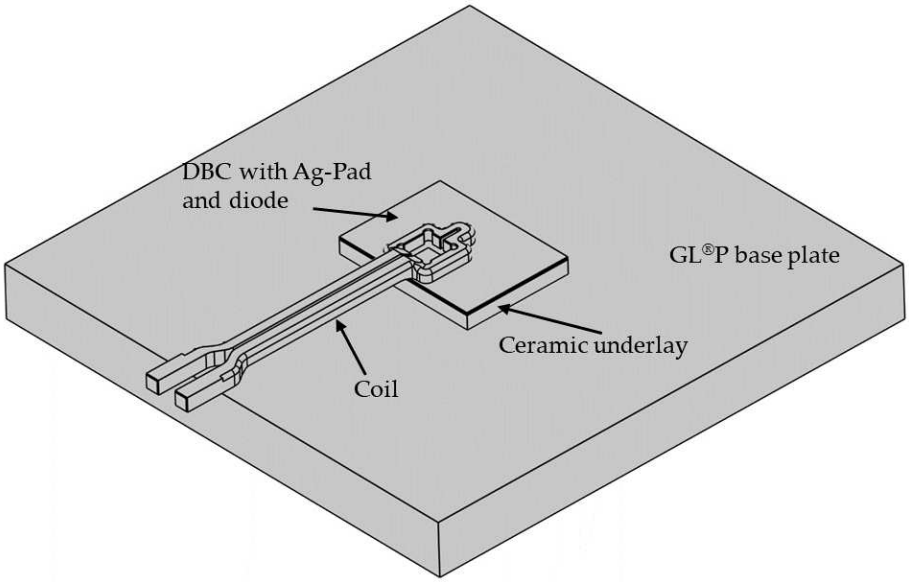

Figure 3. Geometric model of simulation (air box hidden).

Table 2. Material parameters for the FEM. T represents the temperature for temperature-transient values with $c_{Air} = 1047.64 - 0.37 \cdot T + 9.45 \cdot 10^{-4} \cdot T^2 - 6.02 \cdot 10^{-7} \cdot T^3 + 1.29 \cdot 10^{-10} \cdot T^4$ and $\lambda_{Air} = -0.00227583562 + 1.15 \cdot 10^{-4} \cdot T - 7.90 \cdot 10^{-8} \cdot T^2 + 4.12 \cdot 10^{-11} \cdot T^3 - 7.44 \cdot 10^{-15} \cdot T^4$.

Material	**Property**	
	Rel. permeability μ	**Dielectric constant ε_r**
Air	1.0	1.0
Al_2O_3	1.0	9.8
Si (Diode)	1.0	11.7
Cu	1.0	1.0
GL®P	1.0	1.0
SiN	1.0	7.5
	El. Conductivity σ [S/m]	**Heat capacity c [J/(kg · K)]**
Air	1.0	c_{Air}
Al_2O_3	10^{-18}	900
Si (Diode)	$6.4 \cdot 10^{-2}$	700
Cu	$5.998 \cdot 10^{7}$	385
GL®P	10^{-15}	1,140
SiN	0.0	760
	Th. Conductivity λ [W/(m · K)]	**Density ϱ [g/cm³]**
Air	λ_{Air}	ϱ_{Air}
Al_2O_3	27	3.9
Si (Diode)	130	2.329
Cu	400	8.94
GL®P	0.37	2.1
SiN	21.5	3.17
	Reference resistivity ρ @ 293.15 K [Ω · m]	**Resistance coefficient K [1/K]**
Cu	$1.667 \cdot 10^{-8}$	$3.862 \cdot 10^{-3}$

A major focus was set on modeling the material properties of the silver sinter paste ASP 043-04. In the simulation model, the properties of pure silver (as particle matrix with m_{Ag} = 85.3 wt % in the sinter paste) and the organic components (m_o = 14.7 wt %) were combined. Since the boiling point of

the organic paste constituents is at T_b = 219 °C, an erratic change of the paste's heat capacity, density and thermal conductivity was assumed at this temperature in addition. For the determination of the corresponding output values, data from the literature [27] as well as measured values of the paste's thermal conductivity were used.

The thermal conductivity of the silver sinter paste ASP 043-04 was determined for three different annealing temperatures. Silver paste bars were printed onto molybdenum sheets using stencil printing. The samples had a total area of A_{Ag} = 50.0 × 5.0 mm², the bar thickness was h_0 = 500 µm. The printed bars were pre-dried for t = 10 min at T = 110 °C on a hot plate in air. After drying, thickness values in the range of 421 µm ≤ h_1 ≤ 475 µm were measured. Before the heating process, a pressure of p = 10 MPa was applied to all samples. The pressure was kept constant during the entire annealing process. Depending on the sample, the heating process was performed with a heating rate of ΔT = 10 K/min to different target temperatures (T_1 = 250 °C, T_2 = 350 °C, T_3 = 450 °C). The target temperature was kept constant for all samples for t = 2 min. Afterwards, the sintered silver bars were released from pressure and cooled down in air. After detaching from the molybdenum plate, each sample thickness was determined and the LaTIMA method (Berliner Nanotest GmbH, Germany) was used to measure the thermal conductivity of the samples. The results of the thermal analysis as well as the modeling of the silver layer material properties can be found in subsection 3.1.

The simulation results for multiple process parameter combinations were compared to experimentally gained data using the inductor developed during the simulation trials. Therefore, heating experiments for multiple process parameter combinations according to the simulations were conducted without the application of a bonding pressure. The samples were coated with thermal paint and observed during the inductive heating process using the thermal camera PI 640 (Optris GmbH, Germany). Afterwards, the obtained thermal data was analyzed as well as compared with the simulation data.

2.3. Sintering Setup and Method

The induction generator Sinus 251 (HIMMELWERK Hoch- und Mittelfrequenzanlagen, Germany) with a frequency of up to f_{max} = 1.2 MHz and a maximum power of P_{max} = 25 kW was used as the energy source for the inductive heating experiments of the silver particle layers. The experimental setup resulted in a working frequency of approx. 1 MHz by matching the total capacitance C of the resonant inverter to the fixed inductance L of the induction coil. To measure the alternating current through the coil as well as the frequency, a CWT MiniHF 6 Rogowski coil (PEM, United Kingdom) was used.

In order to apply a bond pressure during the sintering experiments, an inductive test rig was realized. The test rig is designed to allow simplified integration of the inductive equipment consisting of induction coil, high frequency generator, resonant inverter, and electrical wiring. Furthermore, the temperature at the diode surface was monitored by means of a thermocouple during the sintering experiments. Figure 4 presents a detailed view of the design solution for measuring the temperature. The drive unit represents an important aspect of the test rig, since the pressure plate has to perform a fine-controlled movement during the die-attach in order to avoid damage to the components. For this reason, a servomotor with a maximum force of F_{max} = 17 kN and an integrated force sensor (Festo Vertrieb GmbH & Co. KG, Germany) realizes the movement of the pressure plate as well as the pressure control. The induction coil was fabricated using selective laser sintering (SLS) based on the simulation results and assembled in the test rig. The entire system with the major components such as the servo motor, the control cabinet, and the sintering chamber is shown in Figure 4.

Preprints (www.preprints.org) | NOT PEER-REVIEWED | Posted: 26 June 2023 doi:10.20944/preprints202306.1796.v1

(**a**) (**b**)

Figure 4. Photographic images of the experimental inductive test rig: (**a**) Entire system with each important components; (**b**) Sintering chamber with support plate for the DBC substrate.

For the sintering experiments, three experimental series were defined and conducted. For each series, process parameters were varied by means of heating time, current range and bonding pressure, Table 3. The coupling distance between coil and DBC was kept constant among all experiments.

Table 3. Overview of process parameters for three experimental bonding series.

Parameter	Experimental series		
	1	2	3
Coupling distance coil – DBC [mm]	1.0	1.0	1.0
Heating time [s]	25; 30; 40; 50	25; 30; 40; 50	25; 30; 40; 50
Max. Frequency [kHz]	1,024	1,024	1,024
Current range (peak-peak) [A]	1,292 – 1,458	1,287 – 1,459	1,290 – 1,465
Joining pressure [MPa]	20.0	10.0	5.0

2.4. Function Test Method

In addition to the bonding experiments described in section 2.3, function tests of the power electronic components were conducted. Therefore, the same process parameters like in Table 3 were used in order to fabricate the samples. For these investigations, the temperature on the top side of the diodes was measured during the bonding experiments by means of thermocouples. Aim of the investigations was to determine if the diodes were damaged during the inductive bonding process due to the strong electromagnetic field or thermomechanical stress.

After bonding, the samples were subjected to block voltage measurement. Therefore, a test voltage of U_p = 1,000 V was applied to all diodes in a two-point measuring arrangement using a curve tracer and the leakage current I_L was measured. In initial condition, the diodes have a block voltage of U_{block} = 1,200 V. In a fault-free diode, the measured leakage current should be as low as possible. For I_{L_crit} > 25,000 nA, a defect in the diode must be assumed.

3. Results and discussion

Preprints (www.preprints.org) | NOT PEER-REVIEWED | Posted: 26 June 2023 doi:10.20944/preprints202306.1796.v1

3.1. FE Simulation

As stated in section 2.2, the proper modeling of the silver sinter layer properties was a major part of the work on the simulation model. The silver sinter paste consists of two components: the metallic silver particle powder and an organic vehicle that serves as a matrix around the particles und converts the powder into an easily processible paste. As a result, it was necessary to determine the thermal conductivity of the paste as described in section 2.2. The results of the LaTIMA analysis are listed in Table 4. The measured thermal conductivity values attract attention because the values decrease as the annealing temperatures rises. This behavior is unusual for sintered structures because with rising annealing temperatures the porosity in a sintered structure should decrease and thus, the thermal conductivity should rise. It can be presumed, that the sinter layer micro structure has an impact on the measured values, which will be discussed more detailed in section 3.5.

Table 4. Annealing temperature, measured thickness, and heat conductivity λ after annealing of the silver sintering bars.

Sample	Annealing temp. [°C]	Thickness after sintering [µm]	Thermal conductivity λ [W/mK]	Δλ [W/mK]
1	250	177	250	26
2	250	171	247	38
3	350	204	222	30
4	350	226	218	36
5	450	215	197	27
6	450	195	199	28

The resulting thermal dependent material properties of the silver paste were modeled like described in section 2.2. Table 5 specifies the properties of the paste layer. Figure 5 presents the associated modeled properties of heat capacity, density, and thermal conductivity as a function of temperature.

Table 5. Material properties of the silver sinter paste ASP 043-04 for the FE simulation.

Material property	Symbol	Unit	Value
Relative permeability	μ	-	0.999975
Dielectric constant	ε_r	-	7
Reference resistivity @ 298.15 K	ρ	Ω · m	$1.6 \cdot 10^{-5}$
Resistance coefficient	K	1/K	$3.8 \cdot 10^{-3}$

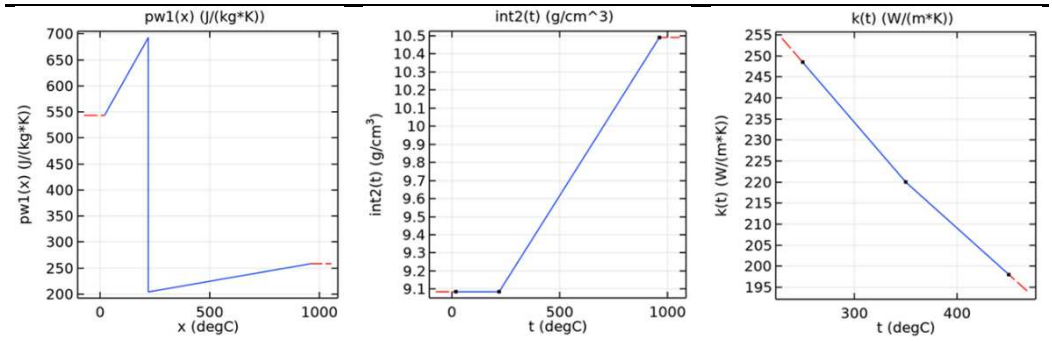

(**a**) (**b**) (**c**)

Figure 5. Temperature-dependent parameters of the particle paste ASP 043-04 used in the simulation: (**a**) Heat capacity, (**b**) Density, (**c**) Thermal conductivity.

With the help of the simulation tools, it was possible to develop a suitable coil geometry for the single-chip bonding tests. The coil has a single convolution, which was subject to numerous iterative adjustments in design in order to focus the maximum heat input to the bonding area on the DBC

Preprints (www.preprints.org) | NOT PEER-REVIEWED | Posted: 26 June 2023 doi:10.20944/preprints202306.1796.v1

substrate. As a result, good homogenization of the inductively generated heat could be realized, so that a uniform and selective heating of the bond zone is possible. An additional circular segment was realized in the rear part of the induction coil's electric line, which allows to arrange a Rogowski coil at the coil, so that the current through the coil as well as the frequency of the alternating current could be measured in the experiments. A CAD image of the coil is shown in Figure 6.

Figure 6. CAD image of the final coil design. Right side: detail of the convolution.

The developed coil was first analyzed virtually regarding its suitability for inductive heating of the stack. Figure 7(a) demonstrates that with a coil current of I = 1,280 A (peak-to-peak), a frequency of the electromagnetic field of f = 1,022 kHz and a heating duration of t_h = 7.0 s. FE simulations showed that sufficient heating (T_{sinter} ≈ 230 °C) of the silver sintering pad can be realized. Areas of the DBC substrate that are below the coil convolution exhibit the highest temperatures, while temperatures decrease significantly with increasing distance from the convolution. Figure 7(b) shows the surface temperature distribution within the silver sinter layer in detail. The temperatures at this location are 206.0 ≤ T ≤ 263.1 [°C]. A hot spot with T_{max} = 319.2 K is located at the lower edge of the DBC substrate because of the induced current accumulating there due to the skin effect. As a result of thermal conductivity, the bottom edge of the silver pad also exhibits a hot spot and the temperatures are decreasing significantly towards the silver pad top side. This temperature inhomogeneity (ΔT = 57.1 K) within the silver pad could be problematic with regard to the formation of a homogeneous micro structure in the bond layer. Nevertheless, the temperatures in the bond zone are sufficiently high for the sintering reaction to take place. In addition, the peak temperatures in the bonding zone of T_{max} = 263.1 °C are not critical concerning the temperature stability of the semiconductor devices, so that no damage to them is to be expected during the induction based bonding process. The very short bonding times are also advantageous in terms of minimizing thermal stress in the diodes. The simulation results were verified by experimentally acquired results from heating tests, performed without the application of a bonding pressure, see section 3.3.

Preprints (www.preprints.org) | NOT PEER-REVIEWED | Posted: 26 June 2023 doi:10.20944/preprints202306.1796.v1

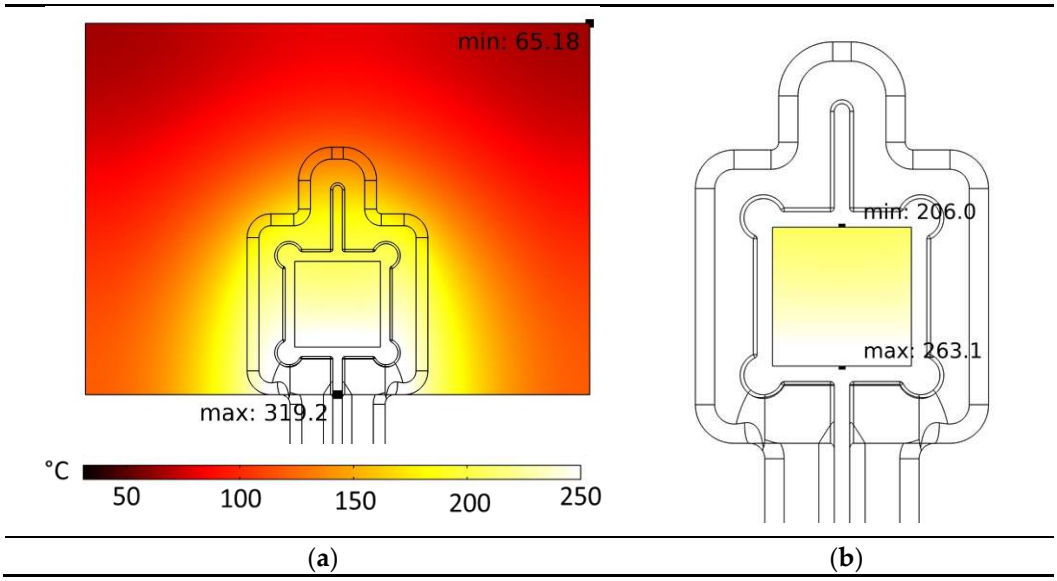

Figure 7. Simulated surface temperature distribution: (**a**) in the stack; (**b**) in the silver sinter layer during inductive heating with a coil current of I = 1,280 A (peak-to-peak), a frequency of the electromagnetic field of f = 1,022 kHz and a heating time of t_h = 7 s.

3.2. Coil Manufacturing

The coil's front part, including the convolution, was manufactured using 3D printing, while the electric connectors were made by manual forming of hollow copper profiles. As 3D printing method, selective laser melting (PROTIQ GmbH, Germany) was applied. Highly conductive copper powder was used for this purpose, which was selectively melted and compacted in the printing process. Thus, the printed coil had an electrical conductivity of about σ_{Cu} = 50 MS/m at a density of ρ_{Cu} = 8.82 g/cm³ [28], which is very close to the corresponding values of pure copper. Then, the coil and the electric connectors were joined by soldering, thus realizing the coil according to the design in Figure 6. In the next step, the coil was installed in the test rig. Figure 8 shows the manufactured coil as it was used for the experiments.

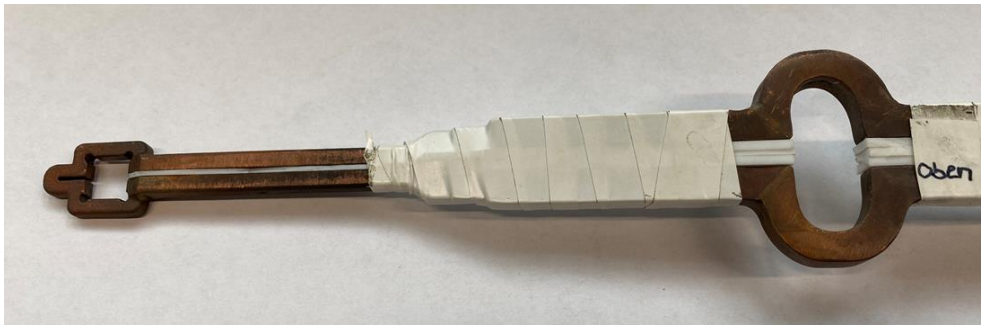

Figure 8. The manufactured coil after simulative optimization.

3.3. Heating Experiments

Heating experiments were carried out by heating the stack with the manufactured coil but without applying a bonding force. In the experiments, coil current ranges of 998 < I < 1,434 [A] (peak-to-peak value), frequency ranges of 1,020 < f < 1,022 [kHz] and heating times up to t_1 = 5.0 s as well as up to t_2 = 10.0 s were applied. The coupling distance in each experiment was s_1 = 1.0 mm. The selection of the process parameters was made with reference to the simulative investigations as described in section 2.3. Temperature measurement on the sample's surface was performed by means of thermal camera. Figure 9 shows an exemplary thermal camera picture of an inductively heated DBC substrate

Preprints (www.preprints.org) | NOT PEER-REVIEWED | Posted: 26 June 2023 doi:10.20944/preprints202306.1796.v1

with a printed silver pad on it, which was captured during one of the heating test. This temperature measurement method was used in order to determine characteristic temperature values in the bond zone and in the surrounding DBC substrate area. A diode was not placed on the pad during the heating tests.

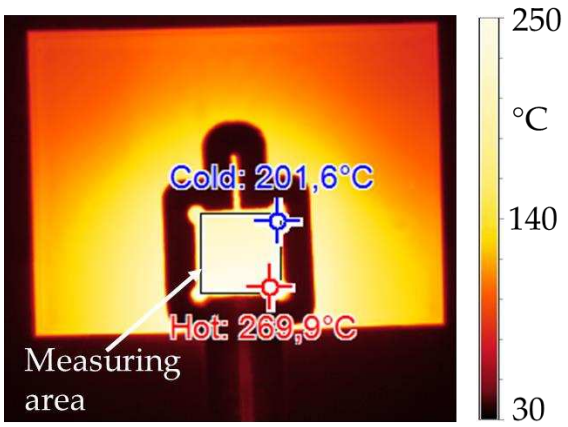

Figure 9. Thermal camera picture captured during the pressure-less inductive heating (frequency of electromagnetic field f = 1,022 kHz, current through coil I = 1,280 A, heating time t = 7.0 s) of a DBC with a printed and pre-dried silver pad. The measuring area corresponds to the position of the diode during the sintering experiments.

From the measured temperatures, it can be observed that the hottest area is a wedge-shaped area inside or directly below the coil convolution. Thus, most of the heat is generated in the bond zone. Areas outside of the convolution are significantly less heated. It can be stated that the experimentally determined heating pattern largely matches the simulated one (Figure 7). For a more precise comparison of the results, the process parameters from Table 6 were used in both, experiments and simulations, and the mean value of the surface temperature of the silver pad was measured and simulated, respectively. The resulting temperature-time graphs were plotted against each other as well as the absolute deviation of the temperature values. Figure 10 shows the corresponding diagrams.

Table 6. Process parameters of the five test series conducted for verification purposes of simulation and experiment. ΔT_{MV}: mean value of the temperature deviation between simulation and experiment. ΔT_{StD}: standard deviation of ΔT_{MV}.

Test series	Process parameter			ΔT_{MV} [K]	ΔT_{StD} [K]
	I_{ind} (peak-peak) [A]	f [kHz]	t_h [s]		
a)	1,140	1,021	10.0	-4.89	4.54
b)	1,280	1,022	10.0	3.62	3.97
c)	1,296	1,022	10.0	1.28	1.91
d)	1,434	1,022	10.0	2.29	5.21

Preprints (www.preprints.org) | NOT PEER-REVIEWED | Posted: 26 June 2023 doi:10.20944/preprints202306.1796.v1

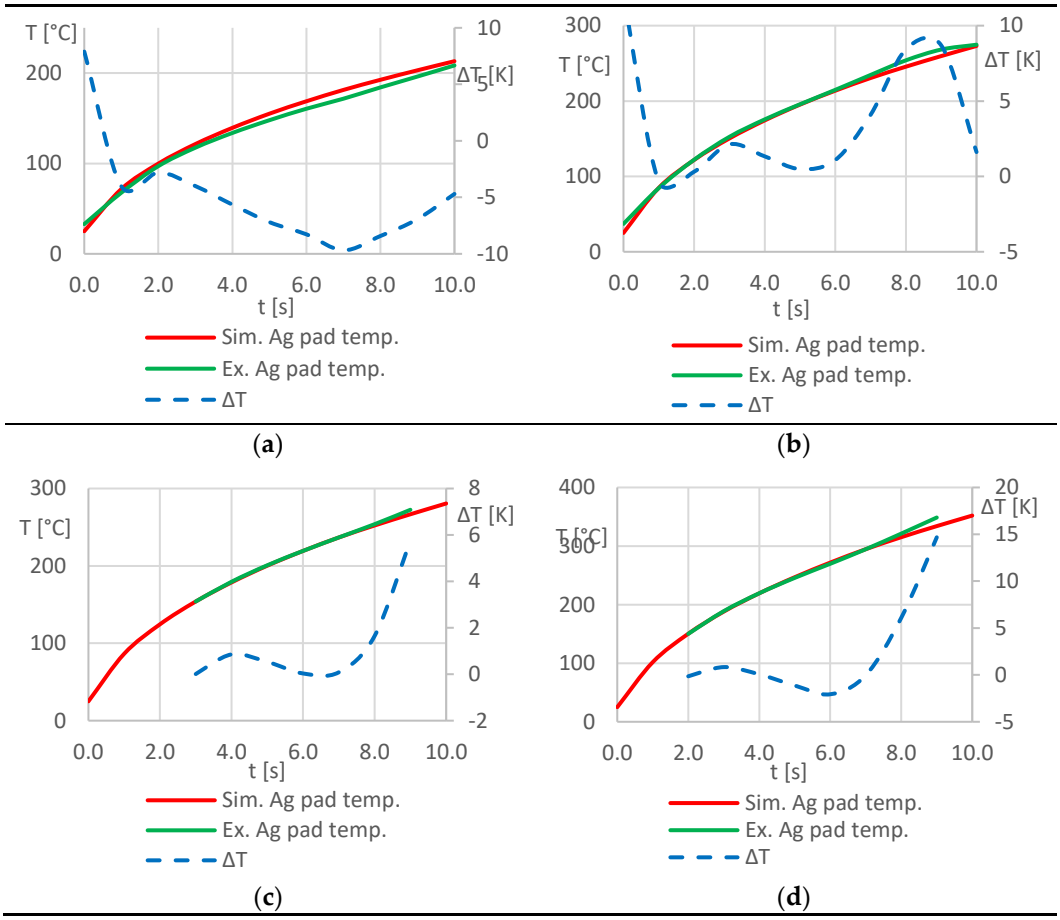

Figure 10. Temperature-time-plots for the silver sinter pad surface from simulation and experiment. Process parameters used for the test series (**a**) – (**d**) according to Table 6.

The diagrams clearly indicate that there is very good matching between simulated and measured temperature values. The mean values of the temperature deviations are $\Delta T_{MV} \leq 5$ K for all considered process parameter combinations. This suggests that the developed simulation model is robust and provides an accurate as well as time and space-resolved prediction of the temperatures in the stack in the investigated temperature range of $25 \leq T \leq 350$ [°C]. In particular, larger deviations between measured and simulated temperature values can be observed at the beginning of the heating process in the experiments in Figure 10(a) and (b), as an initial temperature of $T_{start} = 25$ °C was selected as boundary condition for all simulations but could not be realized at the beginning of the experimental investigations.

3.4. Sintering Experiments

In all test series according to Table 3, diodes were successfully bonded to DBC substrates with induction heating. The produced bonds were firm and of good quality. This proves that induction technology is suitable for the application in die bonding. After initial visual inspection and manual strength testing of the samples, the bonds were characterized in depth by further analysis methods.

3.5. REM Analysis

The bonded samples were cut into cross-sections (cut plane in the middle of the diode) and analyzed by SEM. In the following Figures 11 to 13, an overview of the bonded samples is presented. In the figures, the stack's cross-section consists of the three-layered DBC substrate (DBC-Cu, DBC-Al_2O_3, DBC-Cu), the silver sinter layer and the diode (viewed from bottom to top). In each figure, four specimens from each test series (Table 3) are depicted. For the four samples of each test series,

Preprints (www.preprints.org) | NOT PEER-REVIEWED | Posted: 26 June 2023 doi:10.20944/preprints202306.1796.v1

the bonding pressure and the generator power were kept constant and the bonding time was varied. Because of different bonding times, different maximum temperatures were reached at the end of the heating process. The maximum temperatures are noted in the figures.

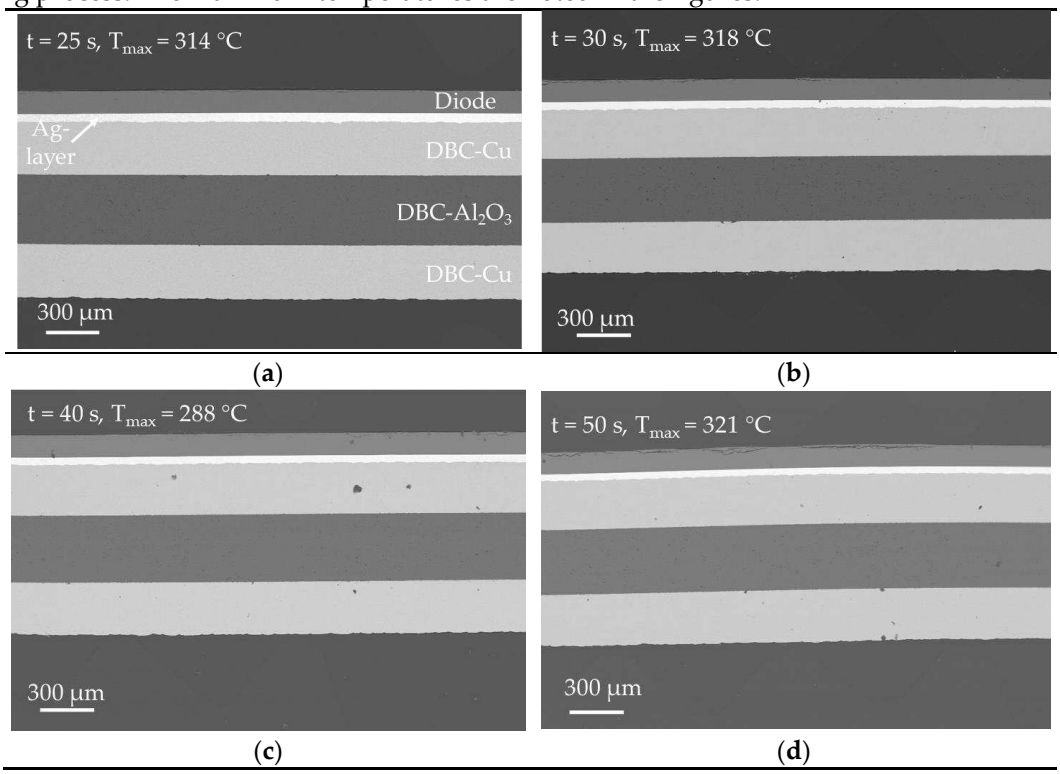

Figure 11. SEM-BSE analysis of the specimens inductively bonded at different process parameters according to experimental series 3 in Table 3. A bonding pressure of p = 20.0 MPa was applied to each specimen. The frequency of the electromagnetic field was $f \approx$ 1,024 kHz in each case. The bonding time was varied among the specimens.

In Figure 11, SEM images of the samples, which were produced at a bonding pressure of p = 20.0 MPa (experimental series 1 in Table 3) are shown. This value was selected as starting point of investigation because a bonding pressure between 20.0 MPa ≤ p ≤ 30.0 MPa is common in current industrial silver sintering processes for die-attach applications. The samples show a very good bonding between DBC substrate, silver layer and diode. The bond interface between DBC substrate and silver sintered layer as well as diode and silver sintered layer is free of defects or voids and the connection between the two components appears to be very firm. Likewise, the densification of the silver sintered layer appears to be very high. Based on the images, no difference in densification of the layers can be observed as a result of the different bonding times or the measured maximum temperature. In addition, almost no defects are visible in the DBC layers, which could be attributed to the bonding process. A few defects can be observed in the copper layers of the DBC substrates, especially in Figure 11(c), but in terms of distribution and size, they do not allow any conclusion to be drawn about a bond process-related formation. Several cracks on top of the diodes are likely the result of the high bonding pressure and the direct contact of the hard ceramic punch and the diode in the bonding process. The damage to the chips is particularly evident in Figure 11(d).

Preprints (www.preprints.org) | NOT PEER-REVIEWED | Posted: 26 June 2023 doi:10.20944/preprints202306.1796.v1

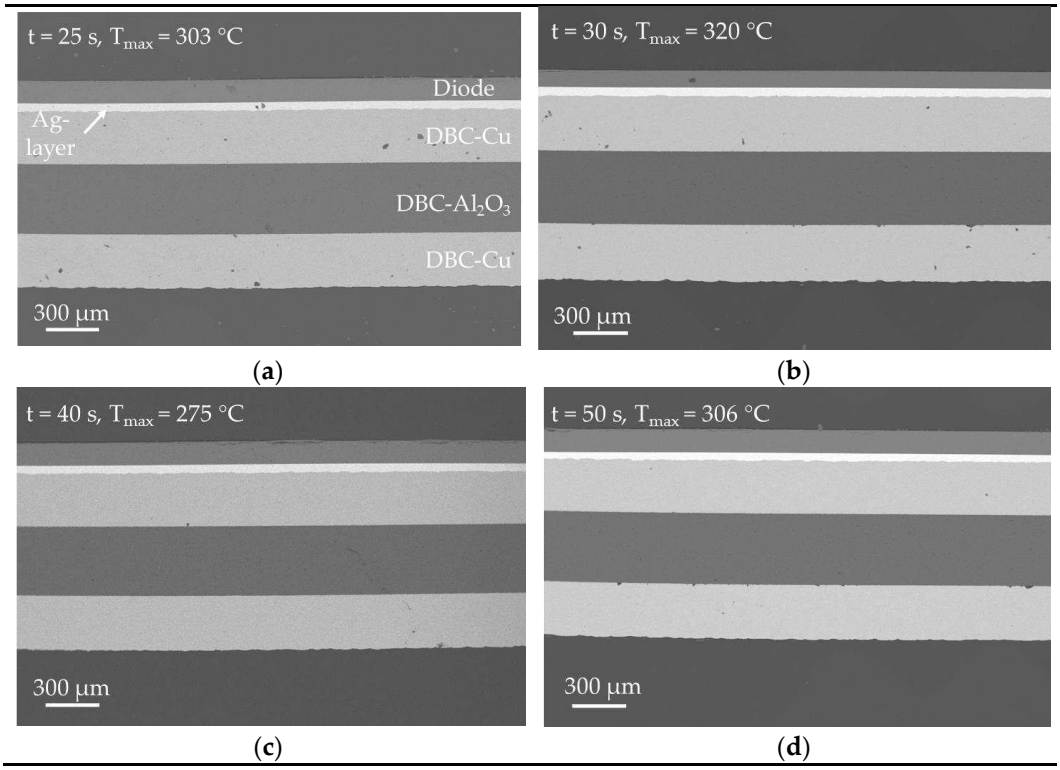

Figure 12. SEM-BSE analysis of the specimens inductively bonded at different process parameters according to experimental series 2 in Table 3. A bonding pressure of p = 10.0 MPa was applied to each specimen. The frequency of the electromagnetic field was $f \approx$ 1,023 kHz in each case. The bonding time was varied among the specimens.

Cross-sectional SEM pictures of the samples, which were produced with a bonding pressure of p = 10.0 MPa (experimental series 2 in Table 3), can be seen in Figure 12. From the images, an excellent bond between the DBC-Ag layer and the diode can be determined for all samples. The densification among all sintered layers in this figure is very high and can be compared to the samples from this experimental series 1 which were produced at a bonding pressure of p = 20.0 MPa. In contrast, it is noticeable that a larger number of defects can be observed in the copper layers of the DBC substrate in the Figures 12(a) and (b). Since the number of defects is much less in Figures 12(c) and (d), which are the samples that were bonded for an even longer time at almost the same temperature, it is assumed that these defects were already present in the DBC substrate before bonding. It is also possible, that the sample was contaminated prior to the SEM analysis and the black dots are dust particles. Furthermore, a few cracks on the diode surface can be observed in Figure 12(c). It becomes evident, that the number of cracks is much lower, in comparison to the samples that were bonded at p = 20.0 MPa. This shows, that a reduction of bonding pressure is beneficial with regard to production safety and quality. A more detailed analysis of the cracks is given later in this section.

Preprints (www.preprints.org) | NOT PEER-REVIEWED | Posted: 26 June 2023 doi:10.20944/preprints202306.1796.v1

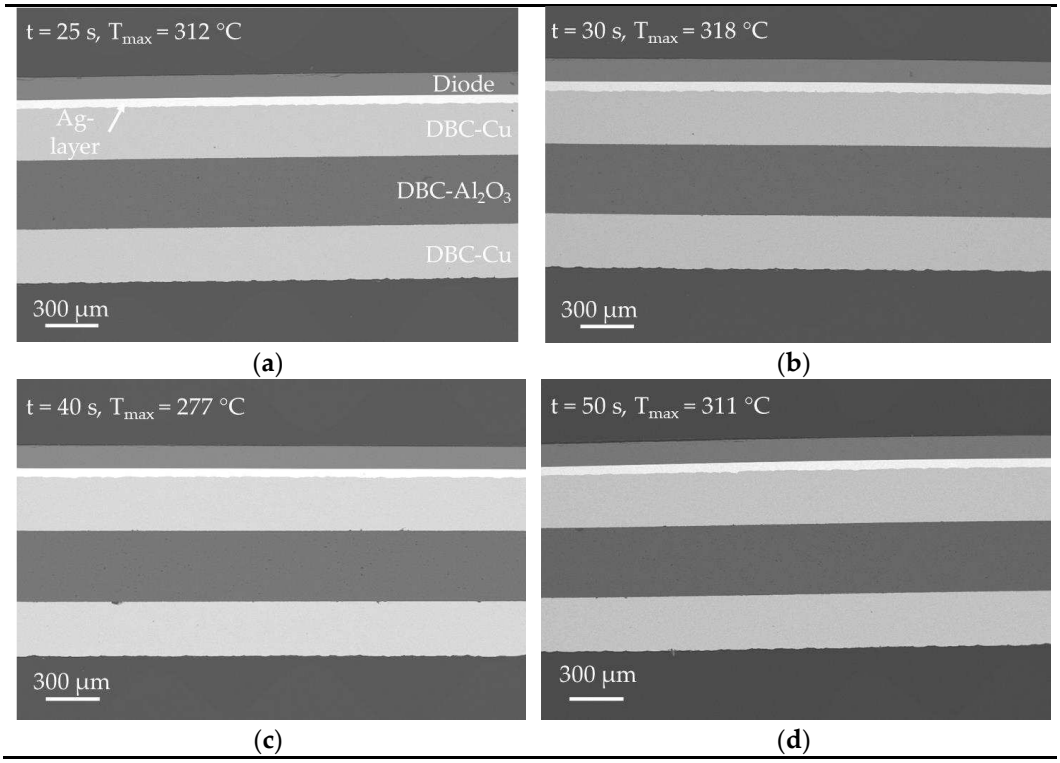

Figure 13. SEM-BSE analysis of the specimens inductively bonded at different process parameters according to experimental series 1 in Table 3. A bonding pressure of p = 5.0 MPa was applied to each specimen. The frequency of the electromagnetic field was $f \approx$ 1,022 kHz in each case. The bonding time was varied among the specimens.

SEM analysis of the samples in Figure 13 shows that a bonding pressure of p = 5 MPa is already sufficient to produce high quality bonds between DBC substrate and diode. The morphology of the bond layers is identical to the previously analyzed samples and the bond to the diode as well as the DCB-Cu-layer is very well established. Several defects can be observed in Figure 10(c) at the interface between DBC-Al_2O_3 and the bottom DBC-Cu layer. However, these are presumably a result of the manufacturing process of the DBC substrate. Almost no cracks in the diode could be found for the samples bonded at p = 5 MPa.

Figure 14 shows a more detailed analysis of the bond zone of the samples from all three experimental series that were bonded for t = 40.0 s according to table 3. In Figure 14 (a), (c) and (e), zoomed-in images of the layer system Diode-silver-DBC-Cu of the sample are shown. The samples were selected because the respective measured temperatures during the experiments were the lowest ($t \approx$ 280 °C) and thus closest to the desired bonding temperature range of 230 < $T_S \leq$ 350 °C. As stated before, for all these samples a very good bonding between the diode and the silver sinter layer can be observed. For all three samples, the thickness of the silver sintering layer is d_{Ag} = 44 µm. With regard to morphology and microstructure of the three silver sinter layers, they appear to be widely identical. However, for the samples bonded at p = 20.0 MPa (Figure 14(a)) and p = 10.0 MPa (Figure 14(c)), several cracks are visible on the diode's top side, which is not the case for the sample bonded at p = 5.0 MPa (Figure 14(e)) where only a single small crack can be observed. Therefore, a bonding pressure of p = 5.0 MPa is sufficient for inductive bonding with the silver sinter paste. By applying this very low bonding pressure, strong and defect-free bonds can be produced and the risk of damaging to the semiconductor components in the bonding process is reduced.

Preprints (www.preprints.org) | NOT PEER-REVIEWED | Posted: 26 June 2023 doi:10.20944/preprints202306.1796.v1

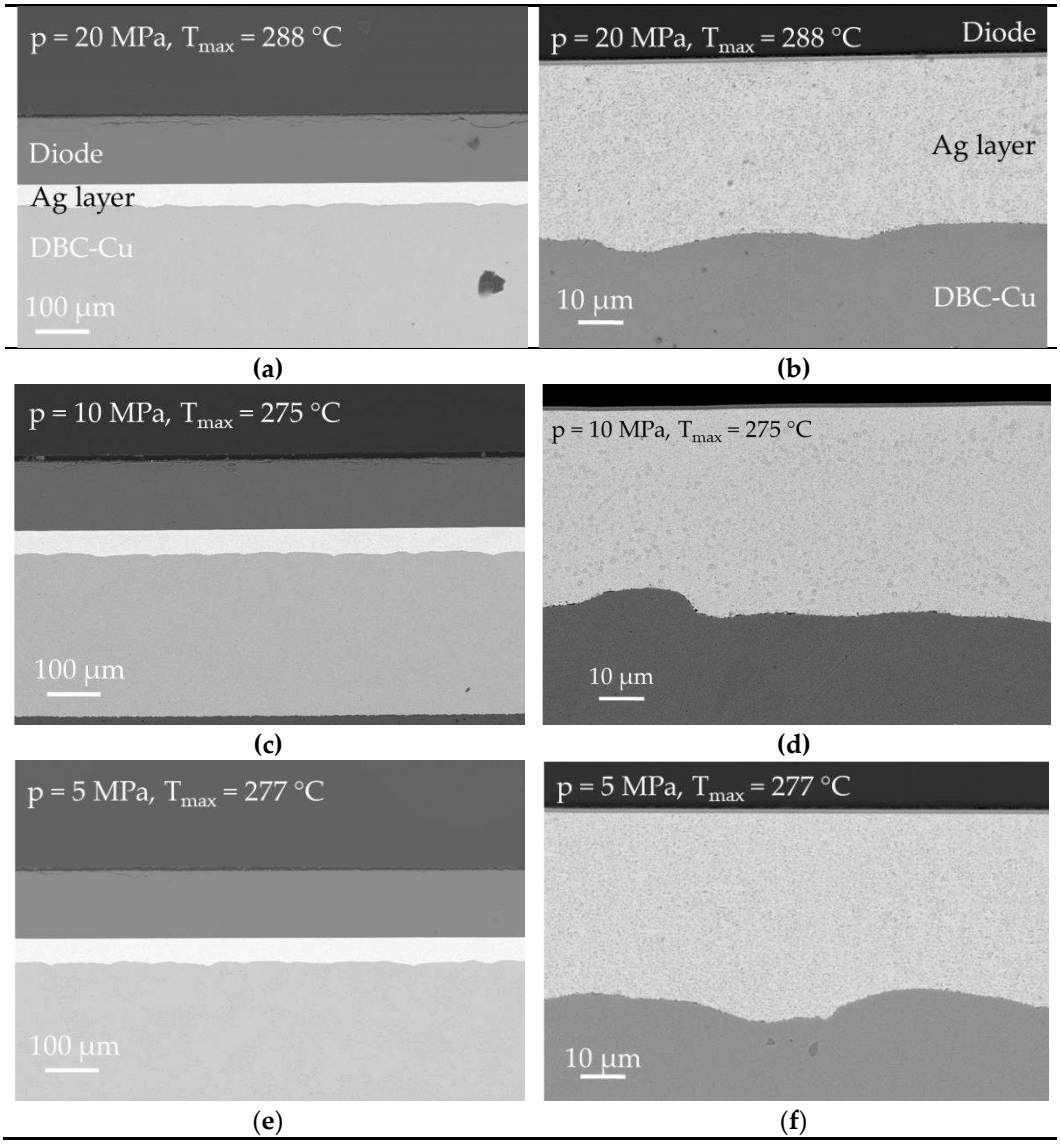

Figure 14. SEM-BSE detail analysis of the bond zone for the specimens inductively bonded at different bonding pressures according to Table 3. Bonding time and frequency of the electromagnetic field were t = 40.0 s and $f \approx$ 1,023 kHz, respectively, for all three samples.

A detailed analysis of the silver sinter layers of the samples is given in the SEM images in Figure 14(b), (d) and (f). It is clear that the densification is very high for all three samples. A certain residual porosity can be observed, but the overall structure and appearance of the layers is very homogeneous, as larger pores cannot be detected. Also, the investigations show that the temperature inhomogeneity during the heating process reported in section 3.3 has no impact on the silver layer morphology, because all investigated samples had an identical appearance throughout the whole cross sections. A more precise quantitative analysis of the layer porosity is to be carried out by means of focused ion beam (FIB) preparation and subsequent SEM analysis in future investigations. Additionally, the pictures prove that the interface between silver layer and diode is defect-free and the two components are tightly bonded. With regard to the very low bonding times and pressures as well as the very high densification of the sintered silver layers, it can be assumed that there is a positive effect on the sintering of the particles with each other as well as to the DBC substrate and diode because of the inductive heating method.

Furthermore, the detached sintered silver bars, which were previously examined by LaTIMA (table 6), were subsequently analyzed by means of SEM. Figure 15 shows the SEM images of one

LaTIMA sample for each annealing temperature. From the figures, it can be seen that the sample which was thermally treated at T_1 = 250 °C (Figure 15(a)) exhibits a clearly visible residual porosity, which is particularly pronounced in the upper and lower thirds of the layer. In the center, there is a comparatively dense zone with hardly any pores to observe. However, the sample is already highly densified. The sintered sample, which was treated at T_2 = 350 °C (Figure 15(b)), shows even less residual porosity, with a few pores primarily agglomerating in the upper third of the sample. Finally, Figure 15(c) shows, that the sample which was treated at T_3 = 450 °C, no longer shows any visible pores. With increasing temperature, a higher densification of the sintered structure can be observed, although a sufficiently high densification of the structure can already be observed at a sintering temperature of T_1 = 250 °C.

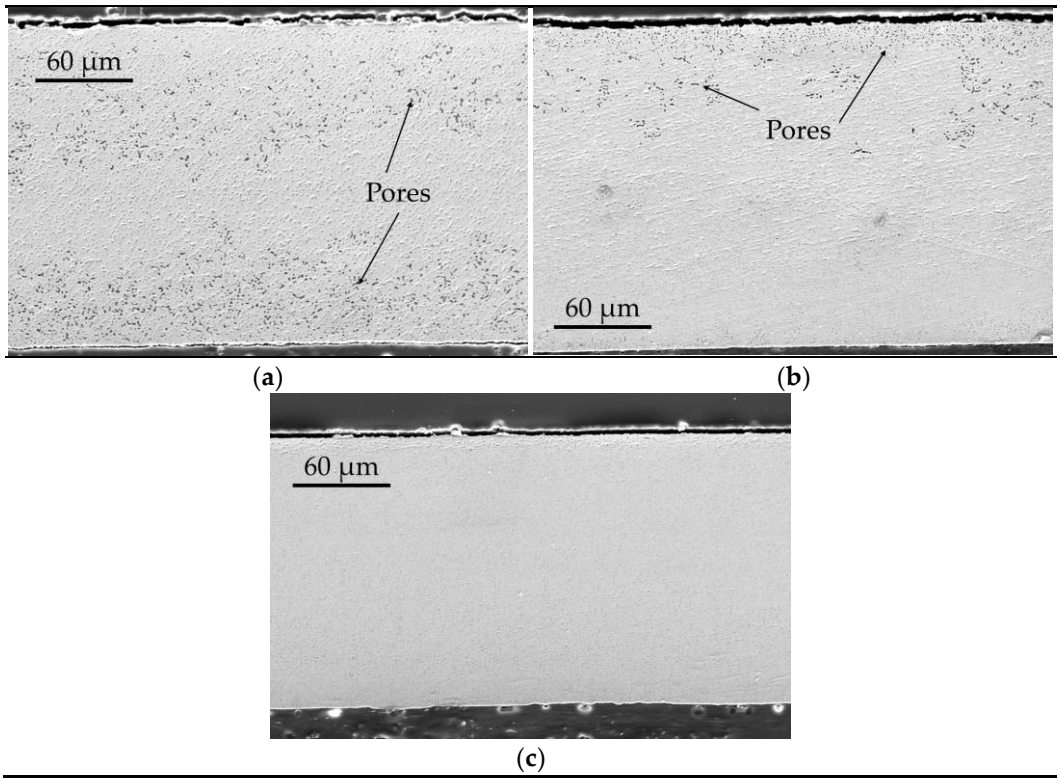

Figure 15. SEM analysis of the detached silver sinter layers thermally treated at different temperatures and analyzed by LaTIMA method according to Table 4. **a**) Sample 2 in Table 4, sintered at T_1 = 250 °C; **b**) Sample 4 in Table 4, sintered at T_2 = 350 °C; **c**) Sample 6 in Table 4, sintered at T_3 = 450 °C.

In section 3.1, the results of the LaTIMA investigations were discussed. For the discussed samples, a decrease in thermal conductivity with increasing sintering temperature could be observed, which is against expectation. With the recently presented SEM analyses of the detached silver sinter layers, a more elaborated discussion of the results is possible. Generally, increasing the densification of a metallic sinter structure is accompanied by an increase in thermal conductivity of the structure. The reason for this is that poorly sintered structures contain gas inclusions which have, compared to metals, a lower thermal conductivity. Thus, as the densification of a sintered structure increases, the pore fraction decreases and the thermal conductivity should increase similarly. This correlation is not true for the samples investigated in this paper. In order to explain this effect, the mean free path of gas molecules becomes important, which is defined as the average distance a molecule travels in a volume until it collides with another molecule and thus exchanges thermal energy. As the pores become smaller into the nanoscale (d < 100 nm) during the sintering process, the mean free path of the gas molecules is greater than the effective space (the pore) in which the gas molecule is confined. This leads to a significant decrease in the number of gas molecule collisions with each other during a constant period and consequently to a strongly reduced thermal conductivity of the gas in the pore. As

 doi:10.20944/preprints202306.1796.v1

a result, the overall thermal conductivity of the nano-porous sintered structure decreases. This effect is known as the Knudsen effect and can be used specifically to produce highly heat-insulating materials [29], [30].

It is possible that this effect is also present in the sintered metallic structures studied here. As the densification of the silver sinter layer progresses, the pores in it become smaller, but there is no complete densification of the sinter structure because there is no liquid metal that can enter the pores and seal them as the sintering process takes place without melting the silver particles. Instead, the particles sinter only by solid-phase diffusion, so that a certain residual porosity remains even after a long time of sintering. Due to the very small dimensions of the pores, they are no longer visible in the SEM images in the Figures 15(a) – (c). However, the thermodynamic influence ~~of these very small pores~~ on the overall thermal conductivity can be clearly seen from the LaTIMA measurements. Since a low thermal conductivity of the sintered layers is not desirable, this aspect of the sintering of silver particles during bonding requires further investigation and optimization.

3.6. Function Test

The results of the function tests by means of block voltage measurement are shown in Table 7. The majority of the diodes endured the inductive bonding process without damage. For 10 out of 12 samples, an average leakage current of I_{L_MW} = 271 nA was measured, which corresponds to a failure-free functionality of the diodes. For sample diode 5, the measured leakage current is I_L = 5,000 nA. According to the measurement norm, this value is still below the limit for defective components (I_{L_crit} = 25,000 nA), but it is notably high compared to the other samples. It is therefore assumed that this sample is also defective.

Table 7. Process parameters and results of leakage current measurement of the investigated bonded diodes. Frequency of the electromagnetic field for all samples was $f \approx 1{,}022$ kHz, coupling distance between coil and DBC surface d = 1.0 mm.

Sample	Bond time [s]	Bonding pressure [MPa]	Max. diode surface temp. [°C]	Leakage current [nA]	Evaluation
1	25.0	5.0	312	275	OK
2	30.0	5.0	318	270	OK
3	40.0	5.0	277	270	OK
4	50.0	5.0	311	250	OK
5	25.0	10.0	303	5,000	Leakage current OK but exceptional high value
6	30.0	10.0	320	280	OK
7	40.0	10.0	275	30,000	not OK
8	50.0	10.0	306	280	OK
9	25.0	20.0	314	250	OK.
10	30.0	20.0	318	300	OK
11	40.0	20.0	288	255	OK
12	50.0	20.0	321	280	OK

Diode sample 7, on the other hand, is clearly defective: a leakage current of I_L = 30,000 nA was measured for it. With regard to the bonding process parameters for this sample (Table 7), no correlation can be found between them and the cause of the damage. Neither the bonding time, nor the bonding pressure or the measured diode surface temperature during the bonding process were exceptional high. It is therefore unlikely that the thermal-electromagnetic stress on the diode in the bonding process led to the failure. For this reason, this sample was subjected to further optical microscopic investigations. The optical microscope analysis of the diode's top metal revealed numerous

Preprints (www.preprints.org) | NOT PEER-REVIEWED | Posted: 26 June 2023 doi:10.20944/preprints202306.1796.v1

damages (Figure 16(a)). In addition, the polyimide guarding at the frame of the diode was also damaged and deformed (Figure 16(b)). All these damages were probably caused by the contact of the SiN punch with the diode during the bonding process. The mechanical impact of the punch on the diode surface presumably damaged the polyimide guarding to such an extent that functionally critical damage to the diode occurred.

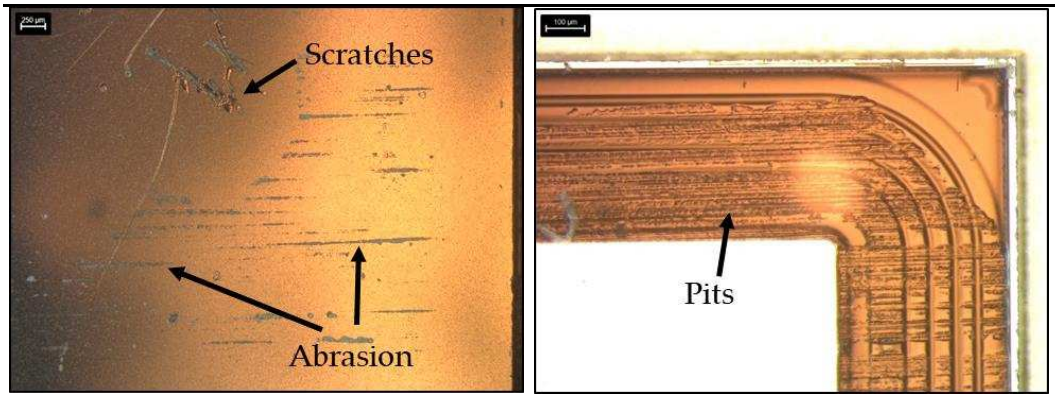

Figure 16. Optical microscope image of sample diode 7 (see Table 7) after bonding. (**a**) Scratches and abrasions on the top metal side of the diode. (**b**) Traces of mechanical influence on the Polyimide guarding of the diode.

Lock-in thermography is a non-destructive testing method for locating damaged areas of a defective diode. Figure 17(a) shows the results of the investigation for the sample diode 7 according to Table 7. In this test method, a pulse current is applied to the diode and it is observed by means of a thermal camera. At the diode's damaged locations, the leakage current flow is very high and as a result, the temperature increases significantly at these locations due to the Joule effect. During the investigations, a hot spot was detected on the right side of the sample diode. The optical microscopic analysis of the corresponding hot spot location is depictured in Figure 17(b). There, a pit in the polyimide guarding can be clearly observed. Like mentioned before, this pit was presumably caused by the mechanical impact of the SiN punch on the diode in the bonding process.

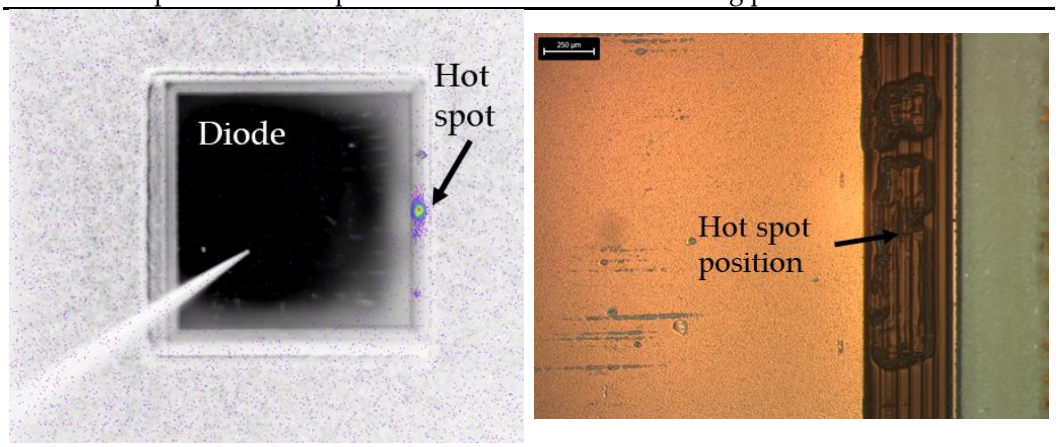

Figure 17. Further analysis of sample diode 7: (**a**) Lock-in thermography of the diode in order to localize the leakage current flow. (**b**) Optical microscope image of the hot spot area.

The results of the function test of the inductively bonded diodes showed that the inductive bonding process did not result in any damage to the semiconductor components. Instead, the observed damage could be attributed to the mechanical impact of the ceramic punch on the diodes' surface. In future experiments, this problem will be overcome by technological adjustments to the test rig, for

example by inserting a buffering polymer film between diode and ceramic punch. Therefore, there are no indications that the inductive bonding process itself did cause any damage to the diodes. Furthermore, evidence has been provided that this technological approach is potentially suitable for industrial application.

6. Conclusion

In this paper, induction heating technology and silver sintering paste as additive material were combined to bond semiconductor components firmly to DBC substrates within very short process times. In preliminary FE simulations, a valid simulation model was developed that allows to simulate the inductive heating process in terms of process analysis and tool optimization. With the aid of the model, it was possible to develop a coil geometry that is adapted to the geometry of the components to be bonded, which allowed for focusing the heat input to the bond zone while keeping the surrounding area less thermally affected. Additionally, it was shown that the strong electromagnetic field does not damage the semiconductor components in the bonding process. SEM analyses of bonded samples showed that excellent bonds could be established between DBC substrate and silver sinter layer as well as silver sinter layer and semiconductor component. The bond interface showed virtually no defects, the bonds are firm and the sinter layers are highly densified. However, further optimizations are necessary with regard to the inductive heating process in terms of coil geometry, position and process parameters in order to ensure homogeneous temperatures in the bonding zone and to avoid hot and cold spots. The bonds need to be further analyzed by means of bond toughness, thermal fatigue resistance and ampacity in order to qualify the process for industrial large-scale production. Furthermore, the results of the investigations need to be transferred and qualified for multi-chip and substrate bonding application in further development steps.

Author Contributions: Conceptualization, P.R., C.H., and M.K.; methodology, P.R., C.H., and M.K.; validation, P.R.; formal analysis, P.R. and S.P.; investigation, P.R., S.P. and R.J.; data curation, P.R.; writing—original draft preparation, P.R. and C.H.; writing—review and editing, M.K. and K.H.; visualization, P.R. and C.H; supervision, P.R.; project administration, P.R., C.H., and M.K.; funding acquisition, C.H., M.K and K.H. All authors have read and agreed to the published version of the manuscript.

Data Availability Statement: Not applicable.

Funding and Acknowledgments: The research project was carried out in the framework of the industrial collective research program (IGF no. 20120 BR). It was supported by the Federal Ministry for Economic Affairs and Climate Action (BMWK) through the AiF (German Federation of Industrial Research Associations eV) based on a decision taken by the German Bundestag.

Conflicts of Interest: The authors declare no conflict of interest. The funders had no role in the design of the study; in the collection, analyses, or interpretation of data; in the writing of the manuscript; or in the decision to publish the results.

References

[1] S. Agarwal, "Status of the Power Module Packaging Industry 2021 - Market and Technology Report 2021," 2021.

[2] C. Rössle and T. Gottwald, "Anforderungen an die Leistungselektronik, Teil 1," *all-electronics.de*, 2016. .

[3] C. Le Bret, Z. Zong, M. Grao Txapartegi, P. Gueguen, H. Lin, and M. Rosina, "From Technologies to Market - Status of power electronics industry 2016," 2016.

[4] N. E. Dowling, *Mechanical Behavior of Materials*, 4th ed. Angshuman Chakraborty, 2013.

[5] K. Guth *et al.*, "New assembly and interconnects beyond sintering methods," *Editor. - PCIM Eur. 2010 - New Assem. interconnects Technol.*, 2010.

[6] J. Yeom *et al.*, "Ag particles for sinter bonding: Flakes or spheres?," *Appl. Phys. Lett.*, vol. 114, no. 25, p. 253103, Jun. 2019, doi: 10.1063/1.5099140.

[7] J. Yan, "A Review of Sintering-Bonding Technology Using Ag Nanoparticles for Electronic Packaging," *Nanomaterials*, vol. 11, no. 4, p. 927, Apr. 2021, doi: 10.3390/nano11040927.

[8] E. Peiner, "Chipmontage mit Drucksintertechnik für Hochtemperaturanwendungen," 2013.

[9] C. Mertens, "Die Niedertemperatur-Verbindungstechnik der Leistungselektronik," TU Braunschweig, Düsseldorf, 2004.

[10] I. Nikitin and K. Pressel, "Mechanical properties of porous silver materials depending on sintering parameters," *THERMINIC 2014 - 20th Int. Work. Therm. Investig. ICs Syst. Proc.*, vol. 2014, pp. 3–6, 2014, doi: 10.1109/THERMINIC.2014.6972536.

[11] A. Hutzler, A. Tokarski, S. Kraft, S. Zischler, and A. Schletz, "Increasing the lifetime of electronic packaging by higher temperatures: Solders vs. silver sintering," in *2014 IEEE 64th Electronic Components and Technology Conference (ECTC)*, May 2014, pp. 1700–1706, doi: 10.1109/ECTC.2014.6897526.

[12] M. Becker, "Neue Technologien für hochzuverlässige Aufbau- und Verbindungstechniken leistungselektronischer Bauteile," Technischen Universität Chemnitz, 2015.

[13] T. G. Lei, J. N. Calata, G.-Q. Lu, X. Chen, and S. Luo, "Low-Temperature Sintering of Nanoscale Silver Paste for Attaching Large-Area (>100 mm^2) Chips," *IEEE Trans. Components Packag. Technol.*, vol. 33, no. 1, pp. 98–104, Mar. 2010, doi: 10.1109/TCAPT.2009.2021256.

[14] G. Zou, J. Yan, F. Mu, A. Wu, J. Ren, and A. Hu, "Low Temperature Bonding of Cu Metal through Sintering of Ag Nanoparticles for High Temperature Electronic Application," *Open Surf. Sci. J.*, vol. 3, no. 1, pp. 70–75, 2010, doi: 10.2174/1876531901103010070.

[15] M. Wang, Y. Mei, W. Hu, X. Li, and G.-Q. Lu, "Pressureless Sintered-Silver as Die Attachment for bonding Si and SiC Chips on Silver, Gold, Copper, and Nickel Metallization for Power Electronics Packaging: The Practice and Science," *IEEE J. Emerg. Sel. Top. Power Electron.*, vol. 10, no. 2, pp. 2645–2655, Apr. 2022, doi: 10.1109/JESTPE.2022.3150223.

[16] K. Xiao, J. N. Calata, H. Zheng, K. D. T. Ngo, and G.-Q. Lu, "Simplification of the Nanosilver Sintering Process for Large-Area Semiconductor Chip Bonding: Reduction of Hot-Pressing Temperature Below 200 °C," *IEEE Trans. Components, Packag. Manuf. Technol.*, vol. 3, no. 8, pp. 1271–1278, Aug. 2013, doi: 10.1109/TCPMT.2013.2261439.

[17] L. M. Chew, T. Stegmann, E. Schwenk, M. Dubis, and W. Schmitt, "A new development of direct bonding to aluminum and nickel surfaces by silver sintering in air atmosphere," *Proc. - Electron. Components Technol. Conf.*, vol. 2019-May, pp. 87–93, 2019, doi: 10.1109/ECTC.2019.00021.

[18] B. D. Sosnowchik, R. G. Azevedo, D. R. Myers, M. W. Chan, A. P. Pisano, and L. Lin, "Rapid silicon-to-steel bonding by induction heating for MEMS strain sensors," *J. Microelectromechanical Syst.*, vol. 21, no. 2, pp. 497–506, 2012, doi: 10.1109/JMEMS.2011.2179013.

[19] H.-A. Yang, C.-W. Lin, C.-Y. Peng, and W. Fang, "On the selective magnetic induction heating of micron scale structures," *J. Micromechanics Microengineering*, vol. 16, no. 7, pp. 1314–1320, Jul. 2006, doi: 10.1088/0960-1317/16/7/028.

[20] C. Hofmann, A. Fröhlich, and M. Wiemer, "A Novel Method for MEMS Wafer-Level Packaging: Selective and Rapid Induction Heating for Copper-Tin SLID Bonding," *Transducers 2019 - EUROSENSORS XXXIII; Solid-State Sensors, Actuators Microsystems*, vol. 20, p. 4, 2019.

[21] C. Hofmann *et al.*, "Localized Induction Heating of Cu-Sn Layers for Rapid Solid-Liquid Interdiffusion Bonding Based on Miniaturized Coils," *Micromachines*, vol. 13, no. 8, 2022, doi: 10.3390/mi13081307.

[22] A. Guyon, E. Biguereau, D. Bouvard, J.-M. Chaix, and S. Roure, "Direct Induction Sintering of Nickel and Silver Powders," in *World PM2016 proceedings: Congress Centre Hamburg (CCH)*, 2016, p. 6.

[23] C. Hofmann *et al.*, "Silver sintering technology based on induction heating for chip level bonding," in *2021 IEEE CPMT Symposium Japan (ICSJ)*, Nov. 2021, pp. 33–36, doi: 10.1109/ICSJ52620.2021.9648867.

[24] P. Rochala, C. Hofmann, M. Kroll, M. Wiemer, and V. Kräusel, "Chip-level bonding for microelectronic components by induction sintering of micro structured Ag particles," 2019.
[25] H. Arnold, "Induktives Chip-Bonden: Innovationssprung für die Leistungselektronik," 2022. https://www.elektroniknet.de/elektronikfertigung/fertigungstechnik/innovationssprung-fuer-die-leistungselektronik.193922.html.
[26] E. A. Olevsky and D. V Dudina, *Field-Assisted Sintering*. Cham: Springer International Publishing, 2018.
[27] A. V. Markin, N. N. Smirnova, I. S. Il'ichev, T. I. Dolinsky, and A. B. Radbil, "Thermodynamic properties of α-terpineol over the range from T → (0 to 345) K," *J. Therm. Anal. Calorim.*, vol. 123, no. 2, pp. 1451–1458, Feb. 2016, doi: 10.1007/s10973-015-5068-0.
[28] "PROTIQ Web page," *https://www.protiq.com/*. .
[29] B. Merillas, J. P. Vareda, J. Martín-de León, M. Á. Rodríguez-Pérez, and L. Durães, "Thermal Conductivity of Nanoporous Materials: Where Is the Limit?," *Polymers (Basel).*, vol. 14, no. 13, p. 2556, Jun. 2022, doi: 10.3390/polym14132556.
[30] D. S. Smith *et al.*, "Thermal conductivity of porous materials," *J. Mater. Res.*, vol. 28, no. 17, pp. 2260–2272, Sep. 2013, doi: 10.1557/jmr.2013.179.